Crossover from semiconductor to magnetic metal in semi-Heusler phases as a function of valence electron concentration

1998 J. Phys.: Condens. Matter 10 1013

(http://iopscience.iop.org/0953-8984/10/5/011)

J. Phys.: Condens. Matter **10** (1998) 1013–1032. Printed in the UK PII: S0953-8984(98)82516-2

Crossover from semiconductor to magnetic metal in semi-Heusler phases as a function of valence electron concentration

J Tobołа†, J Pierre‡, S Kaprzyk†, R V Skolozdra§ and M A Kouacou‡

† Faculty of Physics and Nuclear Techniques, Academy of Mining and Metallurgy, alica Mickiewicza 30, 30-059 Kraków, Poland

‡ Laboratoire de Magnetisme L Néel, CNRS, 166X, 38042 Grenoble, France

§ Chemistry Department, I Franko University, Lviv 290005, Ukraine

Received 10 March 1997, in final form 4 November 1997

Abstract. Experimental and theoretical investigations of intermetallic semi-Heusler compounds (CoTiSn, FeTiSb, CoTiSb, NiTiSn, CoNbSn, CoVSb, NiTiSb) and their solid solutions ($CoTiSn_{1-x}Sb_x$, $CoTi_{1-x}Nb_xSn$) are presented. The physical properties of these systems are found to be mostly determined by the number of valence electrons. Resistivity experiments show that compounds with 18 valence electrons are either semiconductors (CoTiSb, NiTiSn) or semi-metals (CoNbSn). The electronic structure calculations performed on 18-valence-electron systems by the KKR method show nine valence bands below the Fermi level and a gap of order 0.4–0.9 eV. A decrease or increase of the number of valence electrons in CoTiSb, NiTiSn or CoNbSn leads in either case to a metallic state and either ferromagnetic (CoTiSn, CoVSb) or paramagnetic (FeTiSb, NiTiSb) properties. The KKR results concerning 17- and 19-valence-electron systems correspond well with experimental characteristics, except in the case of CoVSb which KKR calculations predict to be a half-metallic ferromagnet, which conflicts with experimental data.

Magnetization and resistivity measurements indicate that semiconductor–metal crossovers occur together with the appearance of ferromagnetism in the $CoTiSn_{1-x}Sb_x$ and $Co_{1-x}Ni_xTiSn$ series, for x near 0.4. This behaviour is discussed in the context of the KKR-CPA results.

1. Introduction

Heusler phases are well known ternary intermetallic compounds, with general formula X_2YZ, where X and Y are transition metals and Z is an sp element. Semi-Heusler phases have the same cubic structure, except that one of the X sites is empty, giving a formula XYZ. Due to the vacant site, the overlap between the d wave-functions is smaller, which gives rise to narrower bands and to the appearance of gaps in the energy spectra. This family of compounds attracted wide interest after the discovery for the NiMnSb and PtMnSb ferromagnets [1, 2] of peculiar electronic structure properties, collectively known as half-metallic ferromagnetism. The half-metallic character arises from the magnetic splitting of the bands, which leads to the occurrence of an energy gap at E_F for down-spin electrons, together with a metallic state for up-spin electrons [3, 4].

In this paper we focus on the physical properties of some XYZ compounds, where the transport and magnetic properties are governed by the number of valence electrons (EC). Compounds such as NiTiSn, CoTiSb with EC = 18 were found to be semiconductors (SC) [5, 6]. In the following, we consider how the electronic and magnetic properties are modified

0953-8984/98/051013+20$19.50

on passing to EC = 19 and EC = 17 systems, by adding (removing) one electron to (from) the different crystallographic sites. We shall see how a crossover from a semiconducting to a metallic state occurs, and how it may be related to the onset of weak ferromagnetism.

Measurements of resistivity and magnetization, as well as band-structure calculations by the Korringa–Kohn–Rostoker (KKR) method, were performed for the following ordered samples: CoTiSn, FeTiSb, CoTiSb, NiTiSn, CoNbSn, CoVSb and NiTiSb. Recently [6, 7], insulator–metal crossovers related to the onset of ferromagnetic ordering were detected in $Co_{1-x}Ni_xTiSn$ and $CoTiSn_{1-x}Sb_x$ solid solutions for x near 0.4. However, the concentration dependencies of the magnetic moments and Curie temperatures are not the same in these two series. In this paper the new series of solutions $CoTi_{1-x}Nb_xSn$ is also described, where the substitution is at the Y site, and compared with the previous $Co_{1-x}Ni_xTiSn$ and $CoTiSn_{1-x}Sb_x$ series. As will be shown, the variations of the physical properties with concentration are again different, as it is not equivalent to add one electron to the X site (filling the d shell of Co), to the Y site (enhancing the density of d states at this site), or to the Z site. In order to get a deeper insight into the influence of alloying on electronic structure, band-structure calculations were performed for the above-mentioned alloys using the KKR method with the coherent potential approximation (CPA). As far as possible, the ground-state KKR-CPA results will be compared to observed properties, and some interpretations will be proposed for these series concerning insulator–metal transitions and the onset of ferromagnetism.

Table 1. The lattice parameter (at RT), Curie and Curie–Weiss temperatures, spontaneous magnetization at 0 K and effective paramagnetic moment (per Co/Fe atom), or constant paramagnetic susceptibility (emu mol^{-1}) for XYZ semi-Heusler compounds. The crystallographic positions of inequivalent atoms in the unit cell can be easily derived, since the chemical formula is written as XYZ, where X is at (0, 0, 0), Y is at (1/4, 1/4, 1/4) and Z is at (3/4, 3/4, 3/4) in the unit cell.

Compound XYZ	a (Å)	T_C (K)	$M(0)$ (μ_B)	θ_p (K)	μ_{eff}	$10^4\chi_p$
CoTiSn	5.997	135	0.357	176	1.35	—
CoTiSb	5.884	—	—	—	—	1.7
CoNbSn	5.947	—	—	—	—	0.53
NiTiSn	5.941	—	—	—	—	1.3
CoVSb	5.791	58	0.18	75	1.26	0
NiTiSb	5.872	—	—	—	—	1.4

2. Crystallography and physical properties

Let us first describe some structural aspects of Heusler systems. The unit cell of the true Heusler X_2YZ structure (space group: $Fm\bar{3}m$) consists of four inter-penetrating f.c.c. sublattices. If one of the two equivalent sites (0, 0, 0) or (1/2, 1/2, 1/2) (here, occupied by X atoms) is empty, the semi-Heusler XYZ structure (space group: $F\bar{4}3m$) appears [5, 8]. As we see from table 1, d atoms occupy X and Y sites, while metalloids are located at Z positions. The smallest d metal generally occupies the site (0, 0, 0) related to the vacancy site (1/2, 1/2, 1/2). The XYZ systems are far from compact, and thus are subject to lattice instabilities. From a chemical point of view, they can be stabilized only through covalent bonding. Thus they are encountered when Z = Sn or Sb, and then only within a restricted range of peripheral electron number. The ideal valence electron concentration (EC) is 8 or 18 electrons per formula unit, which corresponds to AgMgAs, NiTiSn, ZrNiSn,

CoTiSb, CoNbSn, etc. It leads to the formation of tetrahedral bonds and sp^3 hybridization around the p element and favours bonding between d metals. Semiconducting properties occur for EC = 18 for some of the above-mentioned compounds, and disappear for other values of EC.

As always for Heusler compounds, the physical properties are strongly dependent on the crystallographic order. Disorder generally occurs between d metals, the more so the closer they are in the periodic table. Some atoms may also occupy a vacancy site. For these reasons, all of the samples investigated in the present work were annealed for a long time (one week to one month) at temperatures between 650 and 800 °C. Nevertheless, some atomic disorder is still observed. It is not possible for instance to obtain intrinsic semiconductors in these systems and band gaps cannot be determined properly from transport experiments below 300 K. Similarly, the residual resistivity of metallic phases remains significant.

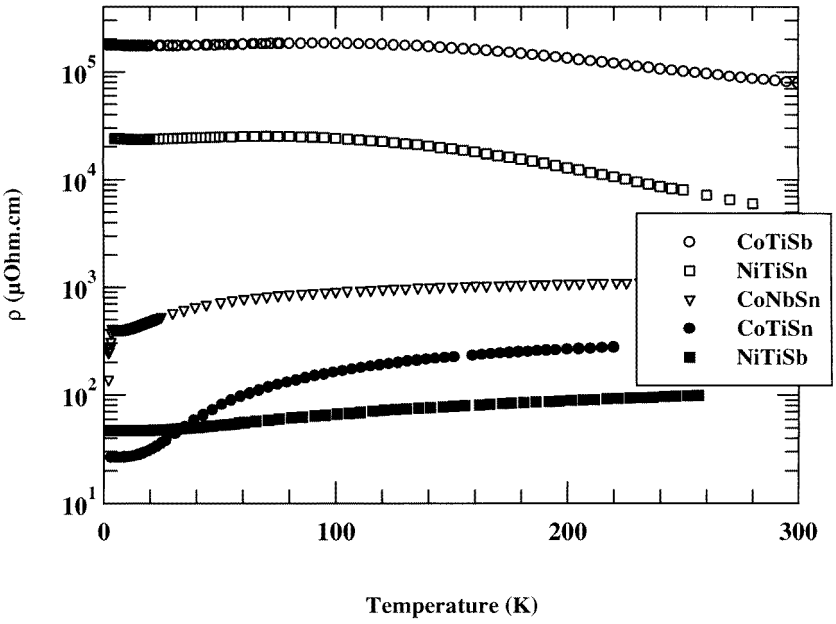

Figure 1. The resistivity for some semi-Heusler compounds.

2.1. The $Co_{1-x}Ni_xTiSn$ series

This series has already been described in previous papers [5, 6]. Here, we recall its basic properties. NiTiSn is a narrow-gap semiconductor ($E_g = 0.42$ eV according to the KKR calculations [9]). Resistivity measurements show that the intrinsic regime is probably not reached even at room temperature. The experimental gap deduced between 200 and 300 K is only 80 meV, much smaller than calculated. This value may be representative of the activation energy of donor or acceptor levels (figure 1). The susceptibility is nearly constant between 15 and 300 K ($\chi = 1.3 \times 10^{-4}$ emu mol^{-1}) (see table 1). Replacing Ni by Co leads first to the narrowing of the gap, then to metallic conduction and finally to the appearance of weak ferromagnetism for a Co (or hole) concentration of about 0.45. No sharp transition occurs between the SC and metallic phases. The limit between semiconducting and metal-

like behaviours was somewhat arbitrarily set to be the concentration at which the temperature derivative of the resistivity changes from negative to positive, or where the low-temperature resistivity is of the order of the (now historical) Mott limit for metallic resistivity, i.e. a few mΩ cm.

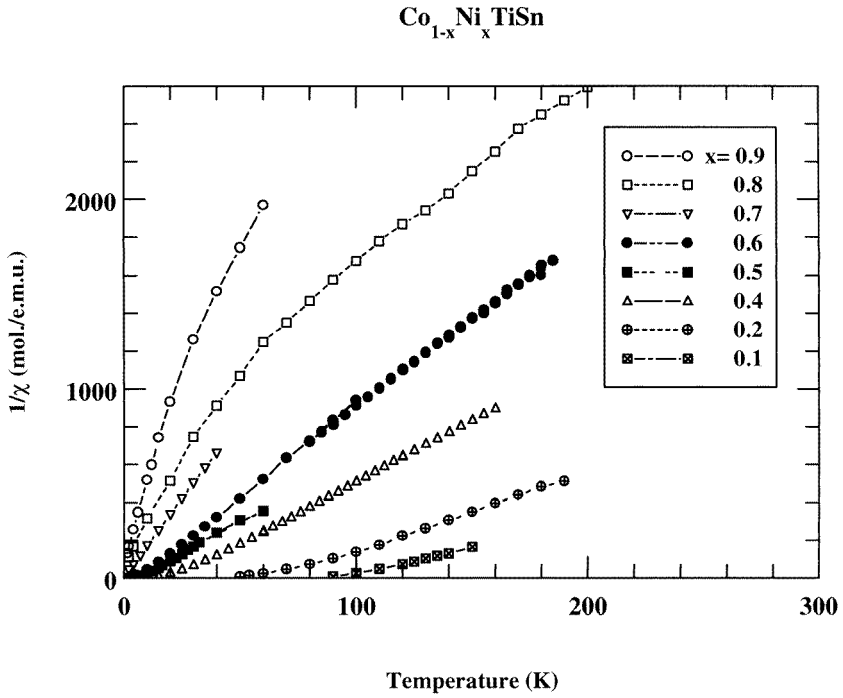

Figure 2. Reciprocal susceptibilities for the $Co_{1-x}Ni_xTiSn$ series.

CoTiSn is a weak ferromagnet, ordering at $T_C = 135$ K, with a moment at low temperature of $M(0) = 0.35\ \mu_B$ (table 2). Co atoms retain a localized moment when diluted in NiTiSn, as shown by the susceptibility of the solutions (figure 2), which exhibit both Curie–Weiss-like and temperature-independent contributions: $\chi = (1-x)C/T + \chi_0$. The Curie constant C per Co ion gives an effective (paramagnetic) moment of Co close to 1.1 μ_B, a value similar to that for pure CoTiSn (1.35 μ_B). Thus the Co paramagnetic moment localizes without a significant change in magnitude when diluted in NiTiSn. In the ferromagnetic range, T_C scales as $M(0)^{1.7}$, which is close to the quadratic behaviour generally observed for localized systems.

2.2. The $CoTiSn_{1-x}Sb_x$ series

Experimental results for this series have already been partly described elsewhere [10]. In this series the solid solution is not continuous: the lattice parameter first decreases regularly on adding Sb up to $x = 0.5$, the phases being metallic. A two-phase region, with two cubic Heusler phases, exists between $x = 0.5$ and $x = 0.6$, then the second semiconducting phase with the smaller lattice parameter continues up to the compound CoTiSb. The SC phase is more compact, which should be ascribed to the bonding mechanism and to the distribution of valence electrons. This SC–metal crossover cannot be a classical Mott transition, since

the SC phase here has a smaller volume than the metallic one and is not magnetically ordered.

The Sn-rich phases order ferromagnetically for $x < 0.5$, but the solutions turn paramagnetic for larger Sb contents. The susceptibility behaviour changes from Curie–Weiss-like in the ferromagnetic range, with an effective moment per Co proportional to the Sn content, to the characteristic behaviour of enhanced paramagnets, with a maximum value in the range 50 to 100 K (figure 3) for SC solutions. A nearly constant susceptibility $\chi = 1.7 \times 10^{-4}$ emu mol^{-1} is observed for the CoTiSb, a result which is close to that ($\chi = 1.14 \times 10^{-4}$ emu mol^{-1}) obtained by Terada *et al* [11]. The magnetic susceptibility of this series as a function of concentration behaves like that of $ZrZn_2$ under pressure [12]. In the ferromagnetic range, T_C is proportional to $M(0)$, a behaviour which was also observed in the metallic solutions between Co_2TiSn and Ni_2TiSn [13].

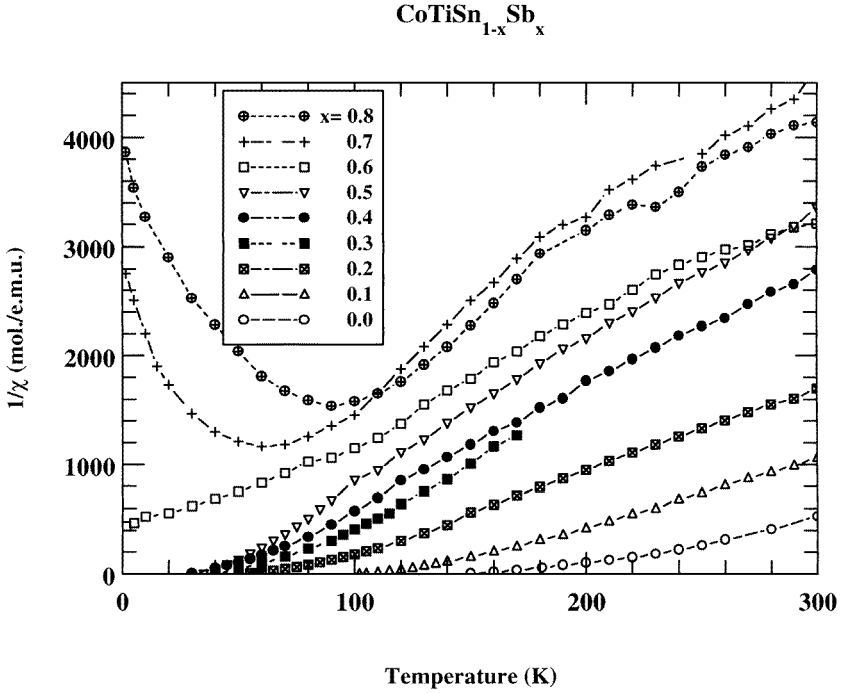

Figure 3. Reciprocal susceptibilities for the $CoTiSn_{1-x}Sb_x$ series.

The resistivity curves of the solutions have a complex behaviour [10]: in the metallic range, the magnetic part of the resistivity becomes larger and larger as the concentration approaches the magnetic–non-magnetic boundary, giving a large T^2-term at low temperature; the S shape of the resistivity is typical of spin fluctuations. For $x > 0.6$, the SC behaviour is recovered.

Thus striking differences are observed between the $CoTiSn_{1-x}Sb_x$ and the $Co_{1-x}Ni_xTiSn$ series. A puzzling feature is that CoTiSb does not order magnetically, and does not even exhibit any localized magnetism (Curie–Weiss susceptibility) whereas Co atoms diluted in NiTiSn do so. A first interpretation would be that an extra electron added to the Z site can be transferred to Co and fills the d shell. We shall see below that this picture is not accurate, and that another interpretation should be given.

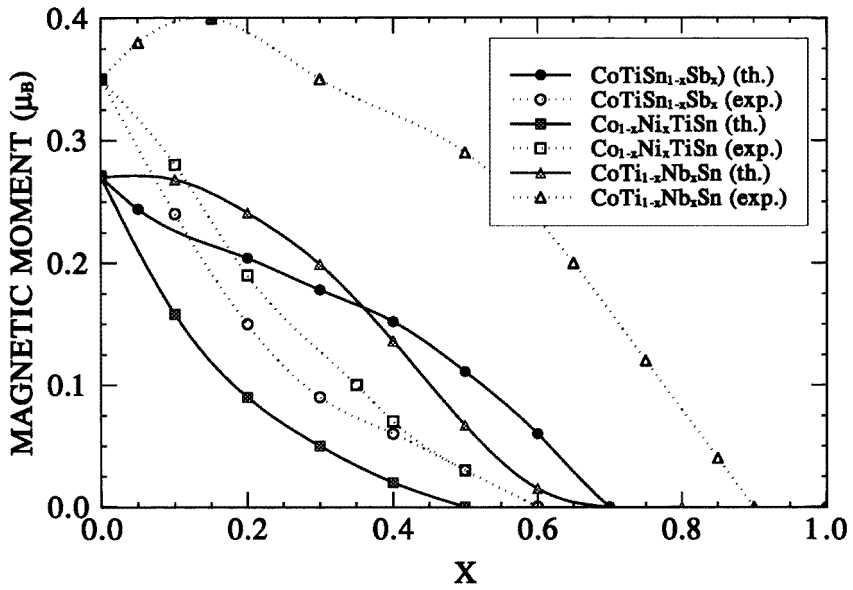

Figure 4. Total magnetic moment variations versus alloy compositions for three isoelectronic series: $Co_{1-x}Ni_xTiSn$ (squares), $CoTiSn_{1-x}Sb_x$ (circles) and $CoTi_{1-x}Nb_xSn$ (triangles). The measured and KKR-CPA points are linked by dotted and solid lines, respectively.

Table 2. Magnetic data for solutions in the $CoTi_{1-x}Nb_xSn$ series.

x (Nb)	T_C (K)	$M(0)$ (μ_B)	θ_p (K)	μ_{eff}
0	135	0.357	158	1.35
0.05	141	0.38	165	1.44
0.15	155	0.40	180	1.51
0.3	120	0.35	151	1.33
0.5	112	0.29	146	1.15
0.65	90	0.20	No CW	—
0.75	23	0.17	—	—
0.85	17	0.12	—	—
0.9	0	0	—	—
1.0	0	0	—	—

2.3. The $CoTi_{1-x}Nb_xSn$ series

A third way to change EC from 17 to 18 is to operate on the third crystallographic site, and to replace Ti by V or Nb. Nb was chosen, since the atomic size of V is smaller than that of either Ti and Nb. In this case, adding a 'd electron' to the Y site should enhance the density of states and correlations on this site. Indeed, the effective moment μ_{eff} per formula unit, θ_p, T_C and $M(0)$ all start to increase with Nb content (table 2, figure 4) up to $x = 0.15$. For $x > 0.15$ all of these quantities decrease, and the ferromagnetism disappears for x between 0.85 and 0.9. The susceptibility of CoNbSn (table 1) is nearly temperature independent and is lower than for other compounds with EC = 18, which may be due to the larger diamagnetic susceptibility of the 4d-metal core. For ferromagnetic samples, the square of the spontaneous magnetization $M(T)$ varies as T^2 for x lower than 0.3, but as

Table 3. The quantities from the band-structure calculations: energy gap E_g, total number of electrons (N_X, N_Y and N_Z), number of d states ($N_{X,d}$, $N_{Y,d}$) inside muffin-tin spheres as well as magnetic moments per formula unit.

Compound	E_g (eV)	N_X	N_Y	N_Z	$N_{X,d}$	$N_{Y,d}$	M (μ_B)
CoTiSn		26.68	20.36	47.83	7.56	1.87	0.28
FeTiSb		25.57	20.38	48.61	6.53	1.96	0.78
CoTiSb	0.95	26.64	20.34	48.52	7.51	1.93	
CoNbSn	0.4–0.6	26.74	38.72	47.82	7.54	2.51	
NbCoSn		39.19	26.42	48.04	2.86	7.44	
NiTiSn	0.42	27.73	20.34	47.87	8.50	1.94	
CoVSb		26.61	21.50	48.41	7.48	2.95	1.00
NiTiSb		27.70	20.33	48.44	8.48	1.96	0.0

$T^{4/3}$ for larger x. This last behaviour was already predicted by Moriya and Kawabata [14] and Lonzarich and Taillefer [15], and attributed to the fluctuations of the order parameter close to the magnetic–non-magnetic crossover.

The resistivity measurements indicate that the metallic character is maintained throughout the series, although the resistivity is much higher for CoNbSn than for metallic CoTiSn or NiTiSb (figure 1). The behaviour observed for CoNbSn implies either a semi-metallic state with a low density of states, or a large atomic disorder which prevents a true semiconducting behaviour. Several CoNbSn samples have been prepared, but even the best one (shown in the figure 1) has a superconducting transition at 3.5 K, a transition temperature which is close to that of Sn. It is probable that some Sn filaments exist between grains and that the stoichiometry of the Heusler phase is not exact. The presence of this spurious phase (undetected by x-rays) may thus explain the metallic-like shape of the resistivity, due to the short-circuit of the primary CoNbSn phase. It may be due to the large difference between the melting points of Sn and Nb, although Co and Nb were first melted together to produce a eutectic with a lower melting point.

Band-structure calculations (see below) show that the inversion of Nb and Co atoms gives rise to a semi-metallic phase instead of a SC one.

2.4. Summary of the experimental results and other compounds

The variation of the ordered magnetic moment $M(0)$ in the three series is plotted in figure 4 as a function of the concentration x (or versus the valence electron number: $17 < \mathrm{EC} < 18$). $M(0)$ decreases continuously and almost at the same rate in the $Co_{1-x}Ni_xTiSn$ and $CoTiSn_{1-x}Sb_x$ series, and the ferromagnetic state disappears for x close to 0.6 (EC = 17.6). For the $CoTi_{1-x}Nb_xSn$ series, the magnetization and the Curie temperature first increase as a function of EC, and then drop to zero for EC close to 17.9. As previously mentioned, the last feature is due to the increase in the d DOS at the Y site which reinforces the magnetic interactions.

Compounds like NiTiSb and CoVSb have 19 valence electrons, and thus a reappearance of metallic conduction may be expected. The magnetic properties of these systems have been investigated by Terada *et al* [11]. NiTiSb is a Pauli paramagnet, with $\chi = 1.56 \times 10^{-4}$ emu mol^{-1} as deduced from measurements between 25 and 250 K ($\chi = 1.37 \times 10^{-4}$ emu mol^{-1} from reference [11]). Resistivity measurements show that this compound is a normal metal. The Debye temperature obtained by a Bloch–Grüneisen fit is estimated to be 220 ± 20 K.

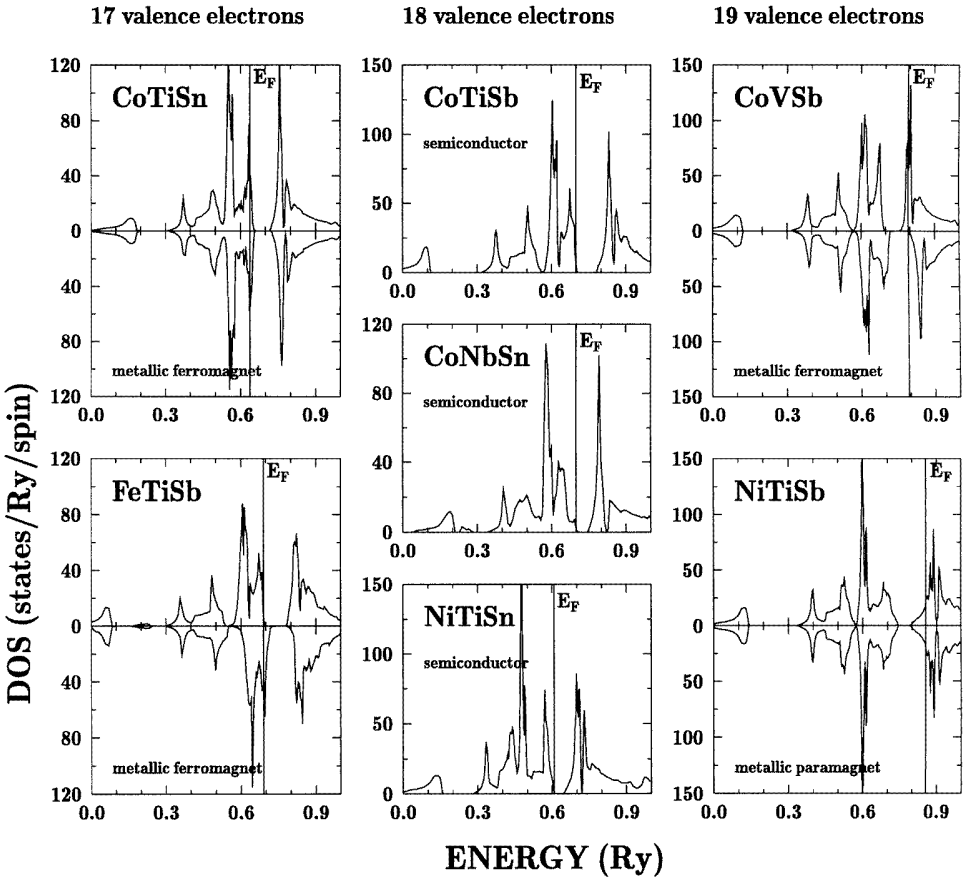

Figure 5. Total densities-of-states spectra of semi-Heusler compounds with various numbers of valence electrons (EC). Each column represents isoelectronic systems. CoTiSn and FeTiSb (EC = 17) are metals, CoTiSb, CoNbSn and NiTiSn (EC = 18) are semiconductors, while CoVSb and NiTiSb (EC = 19) are again metals.

CoVSb is a weak ferromagnet, with $M(0) = 0.18\ \mu_B$, and $T_C = 58$ K [11]. Its effective paramagnetic moment is 1.26 μ_B, close to the values found for CoTiSn and Co diluted in NiTiSn. As for CoTiSn, a fairly large ratio of the paramagnetic to the ferromagnetic moment is observed, which is typical of weak itinerant systems. Finally we observed that FeTiSb (EC = 17) is metallic and exhibits a Curie-like behaviour at low temperatures, but without magnetic order down to 1.5 K.

3. Band-structure studies

We have implemented fully charge and spin self-consistent KKR calculations for CoTiSn, FeTiSb, CoTiSb, CoNbSn, NiTiSn, CoVSb and NiTiSb ordered systems. The computations for $CoTiSn_{1-x}Sb_x$ and $CoTi_{1-x}Nb_xSn$ and the previous ones [9] for $Co_{1-x}Ni_xTiSn$ (with $x = 0.0, \ldots, 1.0$) solid solutions were performed by the KKR-CPA method [16–19]. For compounds as well as for alloys, muffin-tin potentials were constructed within the local spin-density (LSD) approach, using the exchange–correlation part of the von Barth–Hedin

formula [20]. The KKR-CPA self-consistency cycles were repeated for each composition until the difference between input and output potentials was less than 1 mRyd. For the final muffin-tin potentials, the total density of states (DOS), the site-decomposed densities of states (CDOS) and l-decomposed (with $l_{max} = 2$) partial densities of states (PDOS) were computed on a 201-energy-point mesh for the alloys and on a 601-point mesh for the compounds. The integration in $\boldsymbol{k}$-space was performed using 192 small tetrahedra in (1/48)th of the Brillouin zone, applying the method described in reference [21]. The KKR-CPA code contains the generalized Lloyd formula which permits the precise determination of the Fermi energy, using an elliptic contour in the complex energy plane. In our computations the contour contained 48 energy points and the CPA Green function was computed on a mesh of 75 special $\boldsymbol{k}$-points in the irreducible part of the BZ for each of the 48 above-mentioned energy points.

In our calculations the experimental lattice constants were generally used. The KKR-CPA calculations for disordered $CoTiSn_{1-x}Sb_x$ were performed with lattice constants corresponding to the values of CoTiSn and CoTiSb compounds successively. This allowed the influence of the lattice parameter to be checked on the electronic structure, an important feature in this case due to the discontinuity of the solid solution. In the $CoTi_{1-x}Nb_xSn$ series the variation of the cell parameter is quite small (table 1). An empty sphere was added at the (1/2, 1/2, 1/2) position in order to improve the filling factor of the WS cell for filling by non-overlapping muffin-tin spheres (for semi-Heusler systems, when using equal radii, this factor is less than 50%; it increases to 68% on adding extra spheres). The radius $r_{mt} = \frac{\sqrt{3}}{8}a$ was chosen for all non-equivalent atoms in the WS cell, although some numerical trials were done for the CoTiSn compound using various muffin-tin radii for Co, Ti and Sn atoms.

The electronic structure of the end-point compounds was also computed using the KKR-CPA code. Such calculations allow the results obtained by the two methods to be compared and show the DOS characteristics for a vanishing or near-vanishing concentration of one dopant. The limit cases ($x = 0$ and $x = 1$) mean that from the KKR-CPA calculations one may recover for instance the DOS of the Nb atom (one-impurity properties) diluted in the pure CoTiSn, i.e. the $CoTi_{1-x}Nb_xSn$ ($x = 0$) case.

The electronic structure of the present semi-Heusler systems is roughly divided into three groups, according to the number of valence electrons (17-, 18- and 19-electron systems). Figure 5 is a kind of phase diagram, which illustrates the electronic structure of systems and their corresponding ground-state properties. CoTiSn and FeTiSb (EC = 17) are found to be metallic ferromagnets, CoTiSb, CoNbSn and NiTiSn (EC = 18) semiconductors, while NiTiSb and CoVSb (EC = 19) are again metals in the paramagnetic and ferromagnetic state, respectively. From a brief comparison we observe that, even for isoelectronic compounds, the magnetic and transport properties strongly depend on the constituent atoms and their crystallographic positions. From the set of pictures in figure 5, we can easily draw all possible 'paths' between the ordered systems, guessing properties of possible solid solutions. Nevertheless, as observed in our experiments, some phase diagrams do not show a continuous solution. In this paper we focus on the series of solid solutions $CoTiSn_{1-x}Sb_x$ and $CoTi_{1-x}Nb_xSn$, which seem the most attractive for our purposes. The $CoV_{1-x}Ti_xSb$ series has not yet been investigated experimentally and will not be presented in this paper.

3.1. CoTiSn and FeTiSb

The spin-projected DOS picture for CoTiSn (the top-left-hand panel in figure 5, also in reference [9]) shows a weak polarization corresponding to a magnetic moment of about

0.28 μ_B per formula, which is mainly localized on the Co site (0.15 μ_B inside the muffin-tin sphere). The conduction band is formed essentially from d states of Co with some admixture of Sn p states and Ti d states, but part of them are observed above a gap. The DOS for spin up abruptly decreases in the vicinity of the Fermi level, whereas for spin down E_F falls almost precisely at a peak of the DOS. Electronic structure calculations close to the SC–metal limit and close to the magnetic instability are highly sensitive to the determination of the Fermi level. The DOS spectra for CoTiSn (the left-hand column in figure 5) and the position of E_F are deduced from the KKR-CPA method (using the generalized Lloyd formula, when determining E_F). The KKR computations of ordered CoTiSn show stronger polarization of bands and result in magnetic moments both on Co (0.41 μ_B) and Ti (0.30 μ_B) atoms. As stated above, the relevant KKR-CPA calculations for CoTiSn show the magnetization to be of order 0.3 μ_B, mainly due to the magnetic moments at Co sites. Recently, the electronic structure calculations have been performed for the Co_2TiSn and Co_2TiAl Heusler systems with the use of the FP-LAPW and the ASW-ASA methods [22]. The comparison shows that the full-potential LAPW computations lead to a total magnetic moment in agreement with experiment in contrast to the ASW-ASA method, which gives non-magnetic ground states for these systems. This result may be influenced by the use of overlapping spheres (ASA) around atoms, which probably cancel some spin-density contributions. The calculations presented in this paper (using muffin-tin potentials inside non-ovelapping spheres) indicate that CoTiSn and Co_2TiSn [9] are weak ferromagnets with the total magnetic moments 0.28 μ_B and 0.90 μ_B (per Co atom) respectively. These values are close to the experimental data (0.35 and 0.96 μ_B [6]) and to the FP-LAPW results [22].

The electronic structure of FeTiSb (the left-hand column in figure 5) is presented for comparison with that of the isoelectronic CoTiSn. FeTiSb is found to be a metallic ferromagnet with a total magnetic moment per formula unit of 0.78 μ_B; the calculated local magnetic moments at the Fe(X) and Ti(Y) sites are 0.66 μ_B and 0.10 μ_B, respectively. As for CoTiSn, E_F lies at the peak of the spin-down DOS. When comparing the component DOS of these two systems (not drawn here), we notice that the d states of Ti more strongly contribute to the conduction band in the FeTiSb system, resulting among other things in a small magnetic moment on Ti. The integrated partial DOS of the Ti d shell up to E_F (table 2) exhibits a higher value for FeTiSb ($N_{\mathrm{Y=Ti,d}} = 1.96$) than for CoTiSn ($N_{\mathrm{Y=Ti,d}} = 1.86$). This compound indeed exhibits a Curie-like behaviour typical of local magnetic moments at low temperature, with a nearly vanishing Curie–Weiss temperature. However, no magnetic order was detected experimentally down to 1.5 K. As reported in reference [23], the refinement of the diffraction data for FeTiSb seems to show more complex crystallographic structure than the semi-Heusler one (a super-cell or disordered structure). When assuming a disorder on X sites within the X_2YZ-type structure, the KKR-CPA computations show a non-magnetic ground state of $(Fe_{0.5}E_{0.5})_2TiSb$ (E denotes a vacancy), in agreement with the present experiments.

3.2. CoTiSb, CoNbSn and NiTiSn

The KKR studies of semi-Heusler systems possessing 18 valence electrons show the presence of a semiconducting ground state. The basic difference between CoTiSb, NiTiSn and CoNbSn compounds concerns the value of the energy gap E_g, which is biggest ($E_g = 0.95$ eV) for CoTiSb (see table 2). As can be seen from the dispersion curves, bands for CoTiSb (figure 6) and NiTiSn [9] exhibit an indirect Γ–X gap, while E_g for CoNbSn appears between the W and X points in the Brillouin zone.

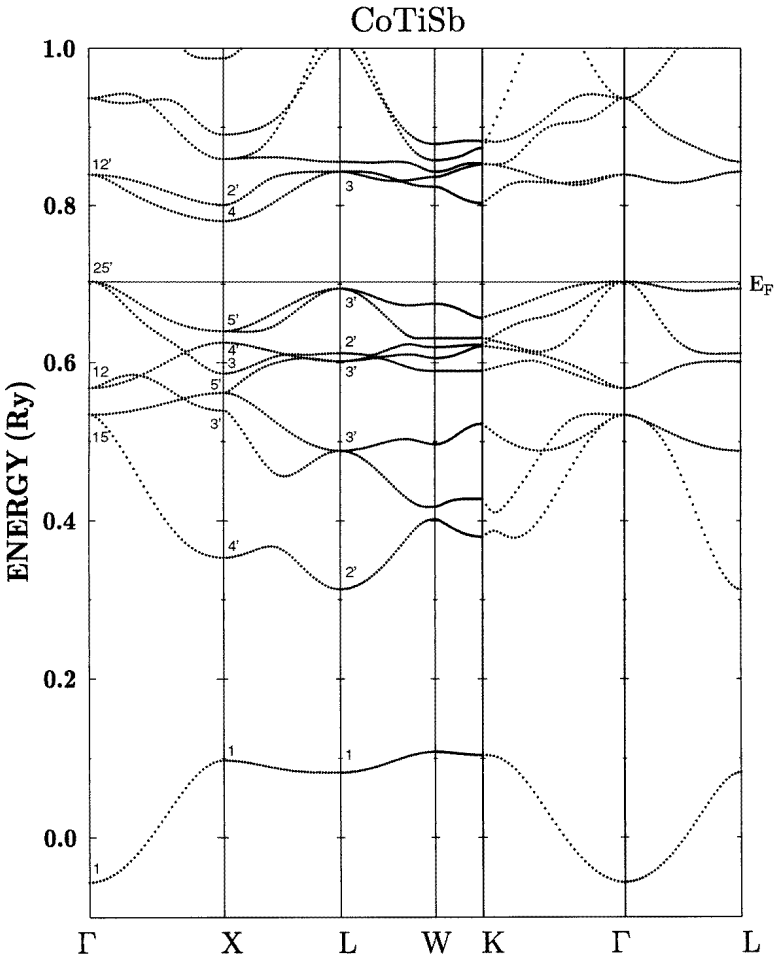

Figure 6. The dispersion curves along high-symmetry BZ directions in the semiconducting CoTiSb. The symmetry labels are assigned according to reference [28].

In this context we recall some limits of the LSD approach in the description of semiconductors. The value of the computed energy gap may be also modified when including the spin–orbit coupling, which is not considered in the present KKR calculations. We expect that upon inclusion of the spin–orbit interaction, the band gaps in semi-Heusler systems may be reduced by about 10–15%, as concluded in reference [24] with respect to the half-metallic PtMnSb.

On the other hand, transport measurements do not give reliable values for the gaps, due to the extrinsic character of the samples (at present, optical measurement results are not available for these systems). Nevertheless, the resistivity values for the three compounds vary in the same sense as the calculated values of the gap (see figure 1 and figure 5).

The CoNbSn compound is near the metal–SC limit, as observed in resistivity measurements. The band-structure studies give an energy gap E_g of the order of 0.4 eV (KKR-CPA) and 0.6 eV (KKR). The disagreement with experiment may arise from the disorder between Co and Nb sites: the KKR computations performed for NbCoSn with

inverted sites (Nb at the X site, while Co is at the Y site) give a semi-metallic state (table 3), with a small DOS at E_F (13 states Ryd^{-1}) mainly due to the Co d contribution.

Both for NiTiSn and for CoTiSb, a dominant character of the electrons (larger mobility, or more donor centres than acceptors) has been observed in the Hall effect. The larger electron mobility may be attributed to the curvature of the valence and conduction bands and to the threefold degeneracy of hole orbitals near the Γ point (the top of the valence band in figure 6), which limits the hole mobility.

For NiTiSn, the main DOS peaks below E_F are principally formed from Ni d states, while above the gap they are due to Ti d states. The situation observed for CoTiSb is slightly different. Here, the gap is two times larger; the electronic spectra deduced from KKR computations also differ from the DOS of NiTiSn. The d states of Co are separated by a gap, and only about 80% of the Co d states are filled below E_F. The main peak of the Co d PDOS is shifted to higher energies, relative to the Ni d PDOS for NiTiSn, due to Co possessing a less attractive potential than Ni. The exact position of the Co d PDOS peak relative to the Fermi energy is also slightly different for CoTiSb and CoNbSn. Moreover, the filling of the d shell of Co in CoNbSn ($N_{\mathrm{Y=Co,d}} = 7.54$) is like that in CoTiSb ($N_{\mathrm{Y=Co,d}} = 7.51$) (see table 3).

From the DOS spectra for the Y and Z sites in the above-mentioned systems (not drawn here), we see, that replacing Ti by Nb and Sb by Sn leads to a higher increase of d states below E_F than the corresponding decrease of p states at the Z site. Consequently, d states from X and Y sites in CoTiSb and CoTiSn are less hybridized than in CoNbSn.

In this comparison we cannot neglect the influence of the Z position on the formation of the energy gap. The degree of hybridization between d states at X and Y sites and p states at the Z site may control the value of the gap. As can be observed from the p PDOS at the Z site, the hybridization is stronger if Z = Sb than if Z = Sn. Thus CoTiSb (with higher electronegativity of Sb) has a wider E_g than NiTiSn and CoNbSn systems. Nevertheless, the d PDOS are very large on both sides of the gap, and hence its value may also be related to the splitting between bonding/anti-bonding wave-functions of transition metals (see the discussion).

3.3. NiTiSb and CoVSb

Adding one electron more to the semi-Heusler EC = 18 compounds, at either the X or the Z position, turns the system metallic, with only one conduction electron per formula unit. When the density of states at the Fermi level is sufficient, as in CoVSb, Stoner's criterion is met and a ferromagnetic ground state occurs. Calculations show that, surprisingly, the magnetization arises from vanadium atoms. This behaviour may be explained by the fact that E_F falls at a high peak of the d DOS for vanadium. The corresponding density for Co is significantly smaller, and thus the local Stoner criterion is not fulfilled.

Both KKR and KKR-CPA methods indicate that the bands are fully polarized; thus CoVSb should be a half-metallic system (the right-hand column in figure 5) with a magnetic moment per Wigner–Seitz cell equal to 1.00 μ_B. The calculated local magnetic moments on Co, V and Sb are found to be -0.02, 1.03 and -0.03 μ_B, respectively. However, this magnetization value is larger than that observed by Terada *et al* [11]. This disagreement may be due to the very rapidly varying DOS in this compound near E_F: from the total DOS for CoVSb, we also conclude that the half-metallic ferromagnetism here is linked to the highly localized conduction states (a large peak of the DOS at E_F). A different ground state may be favoured in a real system; thus an analysis of the total energy variation as a function of polarization should be undertaken. One other reason for the discrepancy

between experiment and theory may be the atomic disorder between Co and V atoms: V has a smaller radius than other 3d metals which occupy the Y sublattice. It is close to that of Co and this may permit greater disorder.

Now, passing to the NiTiSb system, we notice clearly that adding one electron at the X site (Co replaced by Ni) does not have the same effect as increasing the number of electrons at the Y site by replacing Ti by V. The electronic structure of NiTiSb (figure 5) shows striking differences when compared to that of CoVSb. Spin-polarized KKR computations indicate that the ground state of NiTiSb is non-magnetic. In contrast to the Co d states in CoVSb, the Ni d shell in NiTiSb is more or less filled (as in NiTiSn), and the states above the gap are formed with Ti d states. Due to a small value of the DOS at the Fermi level, neither Ni nor Ti atoms in NiTiSb retain magnetic moments. This result is in agreement with magnetization and resistivity measurements, which indicate vanishing magnetization and metallic character in NiTiSb.

3.4. $CoTiSn_{1-x}Sb_x$ and $CoTi_{1-x}Nb_xSn$ alloys

In this section we compare the electronic structure and magnetic properties derived from KKR-CPA computations for the isoelectronic series of alloys $CoTi_{1-x}Nb_xSn$ and $CoTiSn_{1-x}Sb_x$ (figure 7). In the $CoTi_{1-x}Nb_xSn$ series (the right-hand column in figure 7) an increase of valence electron number is brought about by substitution at the Y site by a d element from the next group in the periodic table (Nb), while in the $CoTiSn_{1-x}Sb_x$ series (the left-hand column in figure 7) it is effected by doping the Z site with Sb.

Due to the different origins of the electrons at the two substitution sites, we expect different behaviours of the electronic structure and magnetism for the series, upon alloying the parent compounds. The total magnetic moment (μ_{tot}) variations versus composition are presented in figure 4 for three series (the $Co_{1-x}Ni_xTiSn$ series was investigated in [9]). As in experiments, the variations of μ_{tot} (more or less proportional to μ_{Co}) change non-linearly in all cases. The alloy compositions for which ferromagnetic ordering disappears are also different for the different series. Taking into account the weak ferromagnetism in all of the samples investigated, the critical concentrations found from KKR-CPA calculations are not far from the experimental results. The starting value of 0.28 μ_B for the magnetic moment of CoTiSn at $x = 0$ also slightly differs from the experimental value (0.35 μ_B), which may modify $\mu_{tot}(x)$ dependencies.

First let us consider $CoTi_{1-x}Nb_xSn$ alloys. Here, an interesting observation concerns the concentration-dependent variation of the total magnetic moment, which exhibits a maximum in experiment and a plateau in the KKR-CPA calculations for Nb concentrations of about 0.1–0.2. This is related to an increase in the d states at Y sites, which generates a small induced magnetic moment at this site for $0 < x < 0.2$. It can be seen from the component DOS (the middle and right-hand columns in figure 8), which exhibits some polarization both at the Co site as well as at the Y site (mainly the Ti site) for $x < 0.3$. For higher Nb content, it is mainly the magnetic moment at the Co site that contributes to the total magnetization, which reaches zero for x-values of about 0.6–0.7. Surprisingly, both the gap between the conduction and valence bands in the $CoTi_{1-x}Nb_xSn$ series (the right-hand column in figure 7 and figure 8) and the exchange splitting become smaller as x increases.

For $x > 0.5$ the density of states at the Fermi level subsequently decreases, reaching zero for $x = 1.0$ (an energy gap of about 0.4 eV occurs). This is supported by resistivity measurements, which show an increase of the resistivity in Nb-rich $CoTi_{1-x}Nb_xSn$ samples although, experimentally, CoNbSn appears to be more or less semi-metallic (see section 2.3).

Crystallographic studies have shown that the solid solution was not continuous between

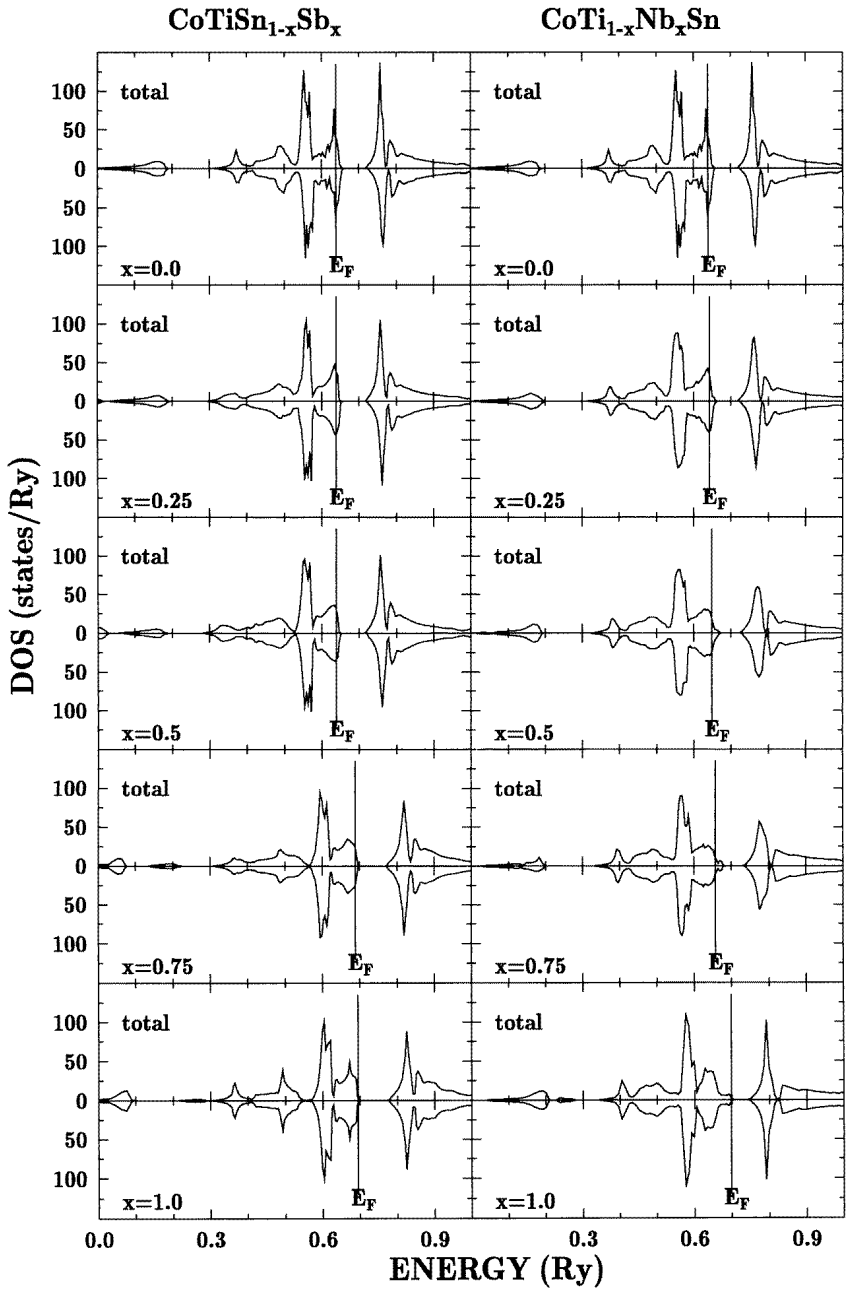

Figure 7. Total densities of states (from the KKR-CPA method) for two disordered series: $CoTi_{1-x}Nb_xSn$ and $CoTiSn_{1-x}Sb_x$.

CoTiSn and CoTiSb. In order to investigate the influence of the lattice parameter on the SC–metal transition, calculations were performed for the $CoTiSn_{1-x}Sb_x$ series with the true parameter (figure 7 and figure 9). The overall DOS shape is not significantly changed (for $x > 0.5$); only a global shift of energies is observed. In the $CoTiSn_{1-x}Sb_x$ series

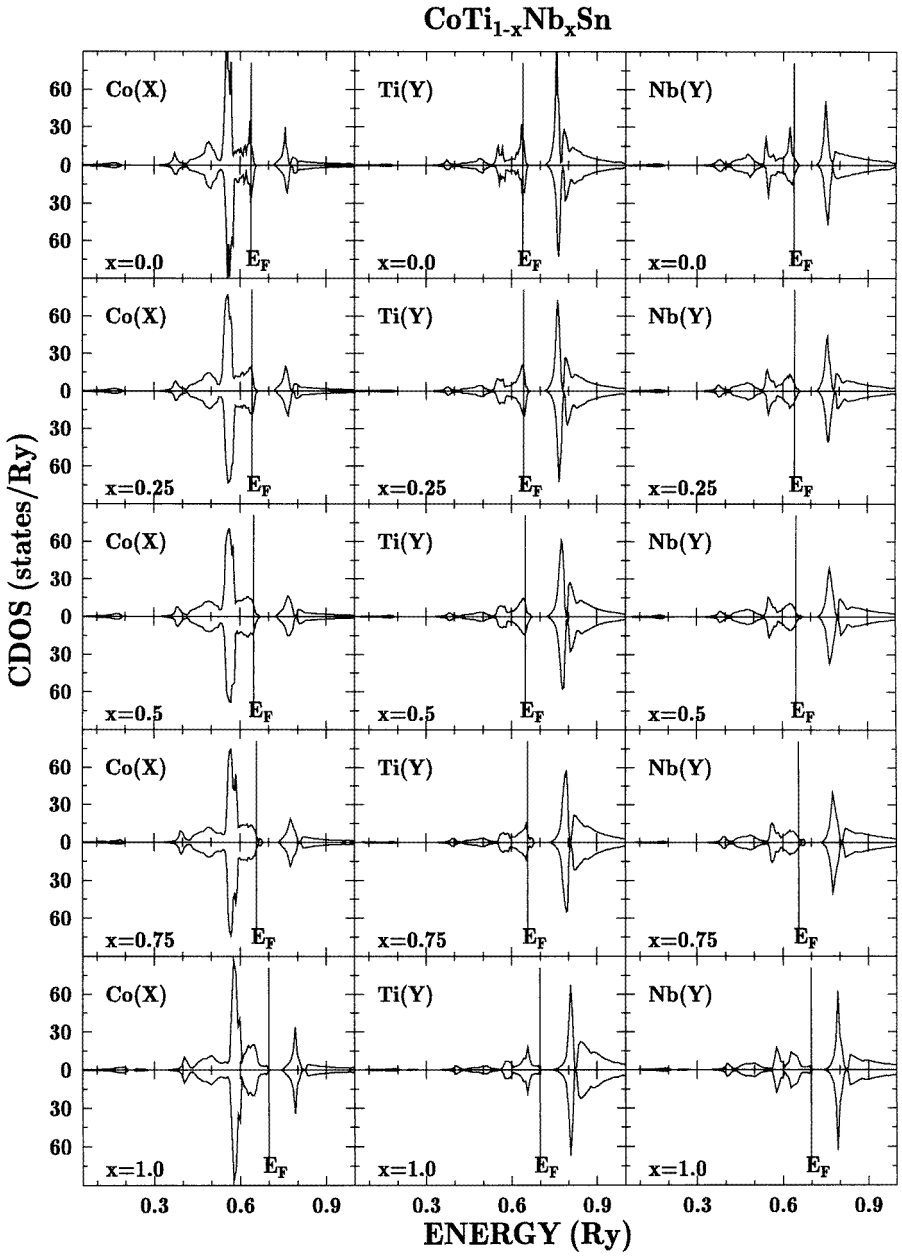

Figure 8. Component densities of states for X and Y sites in the disordered $CoTi_{1-x}Nb_xSn$ series. For borderline concentrations the CDOS of one impurity in the matrix is shown, i.e. Nb in CoTiSn ($x = 0$) and Ti in CoNbSn ($x = 1$).

(oppositely to the previous case), the gap between the conduction and valence bands slightly increases on approaching the CoTiSb compound (the left-hand column in figure 7). The spin polarization continuously decreases, reaching zero for $x \approx 0.7$, which corresponds well to magnetization measurements ($x = 0.6$). Nevertheless, in contrast to the results of the

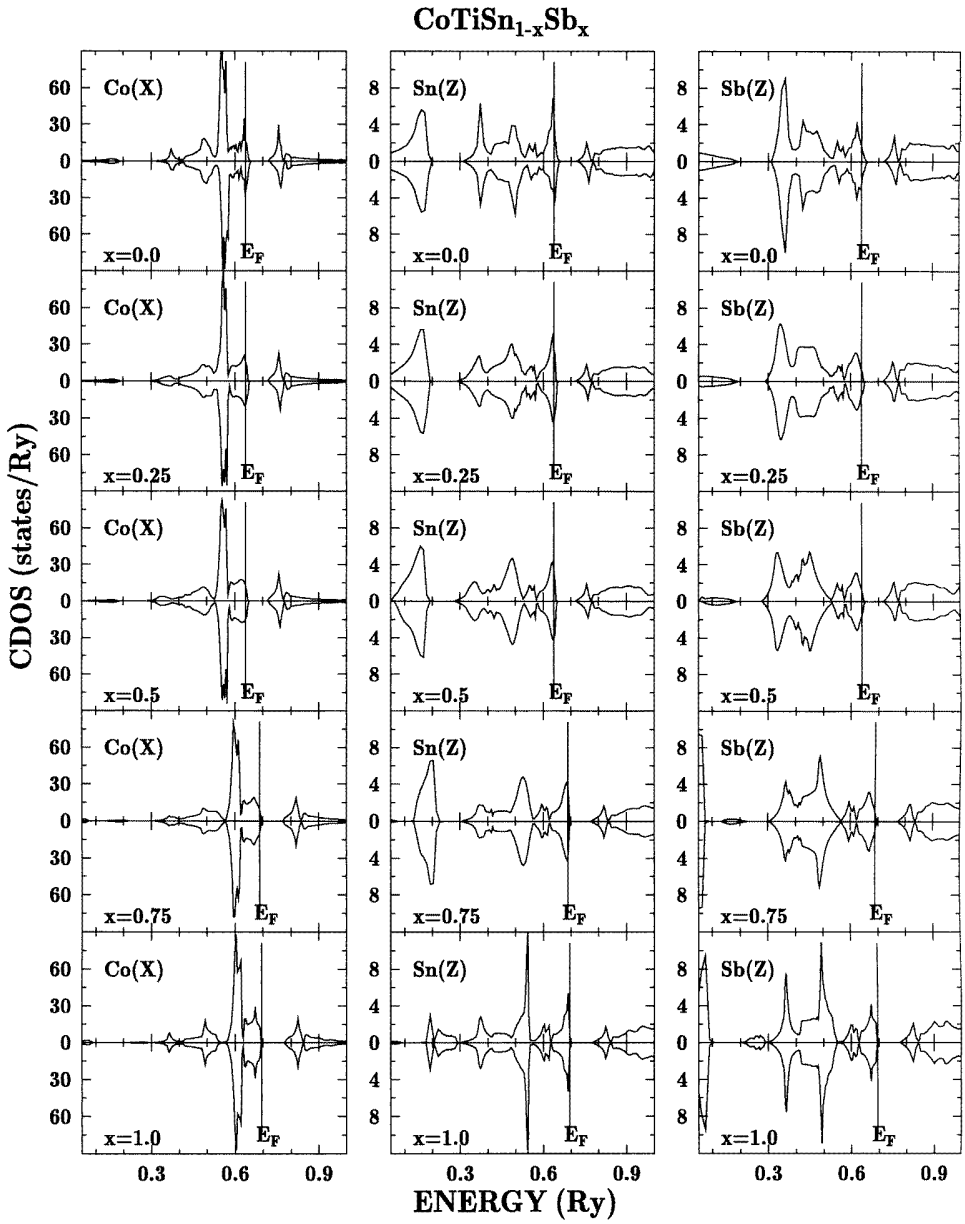

Figure 9. Component densities of states for X and Z sites in the disordered $CoTiSn_{1-x}Sb_x$ series. For borderline concentrations the CDOS of one impurity in the matrix is shown, i.e. Sb in CoTiSn ($x = 0$) and Sn in CoTiSb ($x = 1$).

transport experiments, the crossover to the semiconducting state is not observed in KKR-CPA spectra for intermediate concentrations, mainly due to non-zero contributions of states from Co and Sn atoms (figure 9).

This rigid-band behaviour is a due to eight bands, which are filled for $x = 1.0$, so E_F cannot fall into the gap for $x < 1$. Weakly doped samples probably still have a

semiconducting-like resistivity due to localization arising from the atomic disorder, which will be discussed in the next section.

4. Discussion

Some properties, such as the ferromagnetic–paramagnetic or metal–semiconductor crossovers, can be directly understood from electronic structure calculations, but other results are much less clear and need a more detailed discussion. We will first discuss the transport properties, and next the magnetic properties of these systems.

4.1. Transport properties

We first recall that the gap in the semiconducting phases cannot be properly estimated from our transport experiments below 300 K, due to their extrinsic character. Thus we must rely on the values calculated for the ideal structure within the LSD framework. Nevertheless we observe that the order of magnitude of the measured resistivity goes in the same sense as the calculated value of the gap, both values decreasing from CoTiSb, through NiTiSn, to CoNbSn. This can be simply due to the fact that CoTiSb is better ordered, having fewer impurity states, and CoNbSn is more disordered. One discrepancy between experiments and calculations is the following: when the electron concentration is decreased starting from a SC phase (EC = 18), the resistivity retains a semiconducting-like behaviour (negative temperature derivative) and a large magnitude at low temperatures up to a quite large value for the hole concentration in the lattice. Conversely, in most cases, the CPA calculations indicate that there is a finite DOS at E_F, which implies a metallic state. This should be interpreted in the following way: the CPA calculations do not completely take into account the inhomogeneities in the sample—that is, the different local potentials experienced by carriers due to the chemical disorder—since the environment at an atom is replaced by a mean potential. The resistivity behaviour is indeed caused by the disorder. Anderson and Mott [25] have treated the case of disordered semiconductors, argued for the existence of a mobility edge, and described the mechanism of variable-range hopping (VRH) of carriers, due to localization at the deepest potential wells. In the present system, the typical VRH law: $\ln(R)$ varying as $1/T^{1/4}$ or $1/T^{1/2}$, cannot be observed due to the extrinsic character, but hopping is the common mode of conduction in disordered semiconducting systems [26].

Different types of behaviour are indeed encountered in the present solid solutions. In the case of the $Co_{1-x}Ni_xTiSn$ series, calculations as well as the experimental evidence for a localized moment on Co show that Co levels fall into the former gap of NiTiSn, which is a shortcoming of the rigid-band model. This can explain why the systems remains SC until either a percolation limit is reached, or the Fermi level falls below (for hole doping) the mobility edge, when Co levels collapse into a band. In the case of the $CoTiSn_{1-x}Sb_x$ series, the discontinuity of the lattice parameter of the solid solutions shows that local environment effects must be larger. Conversely, the $CoTi_{1-x}Nb_xSn$ series looks correspondingly more homogeneous and the SC behaviour is indeed rapidly replaced by a metallic state close to the CoNbSn composition.

4.2. Magnetic properties

One first problem is to explain why some compounds present a constant paramagnetism and others a Curie–Weiss behaviour. Moriya and Kawabata [14] have shown that the existence of

strictly localized magnetic moments is not a necessary condition for the existence of Curie–Weiss behaviour. Generally, the Curie–Weiss behaviour has been found to be associated with a sharp peak of the DOS at E_F. Thus we will try to relate magnetic properties to the density of states. We must also explain why localized states of Co diluted in NiTiSn have a small effective moment, why CoTiSb does not show any localized magnetic moments, and also why itinerant magnetic features are observed for narrow bands and, thus, close to a SC–metal transition.

The first observation is that the semiconducting phases NiTiSn and CoTiSb as well as metallic NiTiSb present a susceptibility which does not depend on temperature, whereas CoTiSn and CoVSb present a weak ferromagnetism with a Curie–Weiss behaviour in the paramagnetic range.

Let us first ask what the nature is of the semiconducting phase CoTiSb (charge-transfer, Mott–Hubbard, or another type of semiconductor), and why there is no Curie–Weiss magnetism in this compound. In contrast to the case of Ni in NiTiSn, the d shell of the Co atom is not filled. Electronic structure calculations show (table 3) that there is no more charge transfer from Sb to Co than from Sn to Co in CoTiSn: the number of electrons within the muffin-tin (MT) sphere of Co is the same for the two compounds, and from the partial d DOS the configuration of Co is about $3d^8$. Large electronic correlations within the d shell should maintain a strong intra-atomic coupling. Since Sb p levels are centred well below the gap and have a weak partial DOS on both sides of the gap, we conclude that this gap does not arise only from the charge transfer between Sb and metals. On the other hand, the energy bands (figure 6) show that the splitting between $\Gamma_{25'}$ (occupied t_{2g} states of Co and Ti below E_F) and the unoccupied level Γ_{12} (e_g states above the gap) is about 2 eV. The Co d PDOS is dominant below the gap, and Ti levels dominate above. Thus the gap seems to be due mainly to the hybridization between Co and Ti and the energy difference between bonding and anti-bonding states.

The splitting of d states also indicates that the crystal field around Co is fairly large. In this case, according to Goodenough [27], the spin of the ground state resulting from the crystal field and spin–orbit coupling may be quenched. For a $3d^8$ configuration in a tetrahedral interstice, it has been predicted that the ground state is a non-magnetic singlet (Γ_1 representation), followed by a Γ_4 triplet [27]. This non-magnetic ground state expected for the ionic configuration may tentatively explain why CoTiSb fails to exhibit any Curie–Weiss behaviour, although this ionic picture should be treated with caution due to the strong hybridization with ligands. The hybridization itself, splitting the last occupied bands around the gap, may give rise to this non-magnetic situation.

The constant paramagnetism for other semiconducting phases can be explained as for CoTiSb by a non-magnetic ground state or weak correlations (NiTiSn, CoNbSn), whereas for the NiTiSb metallic phase the more or less uniform Pauli susceptibility is related to a low density of states at E_F.

Conversely, the Curie–Weiss behaviour observed in CoTiSn (or CoVSb) is obviously associated with the presence of a high local density of states at E_F, as revealed by band calculations, and can be rather well understood within the framework of itinerant-electron magnetism. Due to the presence of the gap, only one hole (or electron) participates in conduction and in magnetic ordering, which favours a ferromagnetic type of order. Surprisingly, the magnetic moment in CoVSb is expected to lie on the V atom which has the highest DOS at E_F, rather than on the Co atom. Such a situation should be verified by polarized neutron experiments on single crystals, which is the only way to measure such low ferromagnetic moments.

For solid solutions like $Co_{1-x}Ni_xTiSn$, we pass progressively from one regime to the

other, and the susceptibility can be described by the superposition of a Curie-like term plus a constant susceptibility: $\chi = (1-x)C/T + \chi_0$. The Curie term comes from the rather well localized Co contribution, the other from other d electrons. This is a typical example of localization without a large change in the Co effective moment (1.1 μ_B for Co diluted in NiTiSn, compared to 1.35 for pure CoTiSn). The KKR-CPA band calculations [9] show that the Co d levels tend to form acceptor levels in the gap of NiTiSn (a shortcoming of the rigid-band model), which gives rise to a non-homogeneous magnetism localized at the Co sites. The ferromagnetic order appears when these impurity states are close enough to give rise to a band and thus to a large enough density of states at E_F. A percolation limit can be defined which corresponds to about 0.4 of a hole per formula unit.

The picture of spin quenching by the crystalline field can also explain, together with the weak ferromagnetism expected from the itinerant model, why the magnetic moment is so low for CoTiSn or for $Co_{1-x}Ni_xTiSn$ solutions. Crystal fields and hybridization give rise to a strong breakdown of Hund's rule and to a low-spin state. One interesting feature is that the effective moment remains close to 1.2 μ_B for CoTiSn, for CoVSb and also for some other weak ferromagnets.

Another peculiar feature is the observation of a susceptibility maximum in the $CoTiSn_{1-x}Sb_x$ series close to CoTiSb. Such a behaviour has also been observed for some enhanced paramagnets (YCo_2 for instance) as for $ZrZn_2$ under pressure [12]. Most probably it is related to a pronounced minimum in the DOS at E_F, giving a positive second derivative $n''(E_F)$; the existence of such a minimum is expected as a consequence of the former gap.

4.3. Conclusions and further developments

In summary, many very different behaviours have been observed in these semi-Heusler phases, from semiconductor to metal, from Pauli-like to Curie–Weiss paramagnet, from paramagnetic to ferromagnetic ground state. An overall agreement has been observed between experimental data and electronic band calculations. Some discrepancies remain, since calculations predict for example a ferromagnetic state for FeTiSb (but a non-magnetic state for $(Fe_{0.5}E_{0.5})_2TiSb$) and a fully polarized state for CoVSb which are not observed. Some of the discrepancies may be attributed to the crystallographic disorder in the real lattices and others to the extreme instability of the magnetic polarization near the magnetic–non-magnetic crossover.

Further experiments are planned to investigate in more detail the appearance of magnetism at the Y site, and to follow by substituting for atoms from Ti to Mn the evolution of the ferromagnetic state from the weak-ferromagnet case to the case of complete ferromagnetic polarization and half-metallic behaviour, as found for NiMnSb.

Acknowledgment

This work was partly realized at CNRS Grenoble thanks to a TEMPRA grant allotted to JT by the Rhone-Alpes Region.

References

[1] de Groot R A, Mueller F M, van Engen P G and Buschow K H J 1983 *Phys. Rev. Lett.* **50** 2024
[2] de Groot R A and Buschow K H J 1986 *J. Magn. Magn. Mater.* **54–57** 1377
[3] Kübler J, Williams A R and Sommers C B 1983 *Phys. Rev.* B **28** 1745
[4] Ishida S, Asano S and Ishida J 1984 *J. Phys. Soc. Japan* **53** 2718

[5] Aliev F G, Kozyrkow V V, Moshchalkov V V, Skolozdra R V and Durczewski K 1990 *Z. Phys.* B **80** 353
[6] Pierre J, Skolozdra R V, Gorelenko Yu K and Kouacou M A 1994 *J. Magn. Magn. Mater.* **134** 95
[7] Pierre J, Skolozdra R V and Stadnyk Yu V 1993 *J. Magn. Magn. Mater.* **128** 93
[8] Booth J G 1988 *Ferromagnetic Materials* vol 4, ed E P Wohlfarth and K H J Buschow (Amsterdam: Elsevier Science) p 211 and references therein
[9] Toboła J, Pierre J, Kaprzyk S, Skolozdra R V and Kouacou M A 1996 *J. Magn. Magn. Mater.* **159** 192
[10] Kouacou M A, Pierre J and Skolozdra R V 1995 *J. Phys.: Condens. Matter* **7** 7373
[11] Terada M, Endo K, Fujita Y and Kimura R 1972 *J. Phys. Soc. Japan* **32** 91
[12] Grosche F M, Pfleiderer C, McMullan G J, Lonzarich G G and Berhoeft N R 1995 *Physica* B **206–207** 20
[13] Pierre J, Skolozdra R V and Kouacou M A 1995 *Physica* B **206–207** 844
[14] Moriya T and Kawabata A 1973 *J. Phys. Soc. Japan* **34** 639
[15] Lonzarich G G and Taillefer L 1985 *J. Phys. C: Solid State Phys.* **18** 4339
[16] Kaplan Th, Leath P L, Gray L J and Diehl H W 1980 *Phys. Rev.* B **21** 4230 and references therein
[17] Kaprzyk S and Bansil A 1990 *Phys. Rev.* B **42** 7378
[18] Bansil A, Kaprzyk S and Toboła J 1992 *Applications of Multiple Scattering Theory in Material Science (MRS Symp. Proc. 253)* (Pittsburgh, PA: Materials Research Society) p 505
[19] Kaprzyk S 1997 *Acta Phys. Pol.* A **91** 135
[20] von Barth U and Hedin L 1972 *J. Phys. C: Solid State Phys.* **5** 1629
[21] Kaprzyk S and Mijnarends P E 1986 *J. Phys. C: Solid State Phys.* **19** 1286
[22] Mohn P, Blaha P and Schwarz K 1995 *J. Magn. Magn. Mater.* **140–144** 183
[23] Szytuła A, Tomkowicz Z and Turowski M 1973 *Acta Phys. Pol.* A **44** 147
[24] Continenza A, de Pascale T M, Meloni F and Serra M 1993 *Japan. J. Appl. Phys.* **32** 240
[25] Mott N F 1974 *Metal–Insulator Transitions* (London: Taylor and Francis)
[26] Pollack M and Shklovskii B (ed) 1991 *Hopping Transport in Solids* (Amsterdam: North-Holland)
[27] Goodenough J B 1963 *Magnetism and the Chemical Bond* (New York: Wiley–Interscience) p 67
[28] Bouckaert L P, Smoluchowski R and Wigner E 1936 *Phys. Rev.* **50** 58